Remote response modes on the paced excitable *C. elegans* network

Yu Qian,[1,*] Zhili Chen,[1] Runru Yang,[1] Hongyan Gao,[1] Zhao Lei,[1,†] and Zhigang Zheng[2,3,4,‡]
[1]*College of Physics and Optoelectronic Technology, Baoji University of Arts and Sciences, Baoji 721007, China*
[2]*Institute of Systems Science, Huaqiao University, Xiamen 361021, China*
[3]*College of Information Science and Engineering, Huaqiao University, Xiamen 361021, China*
[4]*School of Mathematical Sciences, Huaqiao University, Quanzhou 362021, China*

(Received 7 April 2024; accepted 12 June 2024; published 2 July 2024)

In paced excitable systems, a traditional viewpoint on signal transmission is that an excitable pacing signal should propagate from the source to its excited neighbors in a sequential rule, which is known as the normal *sequential response mode* (SRM). However, in our present paper, by extensively exploring the response modes emerged on the *paced excitable C. elegans network*, we found that, besides the normal SRM, a response mode that breaks the sequence rule and contains isolated excited clusters or even isolated excited nodes on the propagation path of the response structure can be detected. Such remote response nodes and clusters are excited discontinuously from the source node, forming the phenomenon of the *remote response mode* (RRM). An *effective-driving analysis approach* (EDAA) is proposed to theoretically study the mechanism of the RRM, based on which key role played by the excited nodes possessing nonexcited upstream driving neighbors is confirmed in the formation of the RRM. We further verify the applicability and the universality of the EDAA in identifying the RRM on general paced excitable networks. These contributions are expected to shed light on the study of complex response modes in paced excitable systems and to have great impact in related topics.

DOI: 10.1103/PhysRevResearch.6.033014

I. INTRODUCTION

Since the seminal "small-world" and "scale-free" network models were successively proposed by Watts and Strogatz and Barabási and Albert (see [1,2], respectively), great progresses have been achieved in the field of complex network science. Subsequently, collective behaviors emerged on different types of complex network systems have become the central hot topics under investigation in the fields of nonlinear science and network science. Several typical types of spatiotemporal dynamical behaviors, such as synchronous phenomena [3–6], self-sustained oscillations [7–11], and chimera and chimera-like states [12–16], have been discovered. For example, Zhang *et al.* revealed the explosive synchronization in adaptive and multilayer networks [4]. Fretter *et al.* discussed the topological determinants of self-sustained activities in a simple model of excitable dynamics on graphs [11]. Hagerstrom *et al.* experimentally observed the chimeras in coupled-map lattices [12]. In addition, response dynamics is also an important topic in this field and lots of interesting results have been reported [17–25]. For example, Tolkacheva *et al.* investigated the condition for alternans and stability of the 1:1 response pattern in a "memory" model of paced cardiac dynamics [18]. Chen *et al.* studied the resonant response of forced complex networks and revealed the key role of topological disorder [20]. Grabert and Thorwart exposed the quantum mechanical response to a driven Caldeira-Leggett bath [22]. Wang *et al.* discovered the frequency-dependent response in the cortical network with periodic electrical stimulations [24].

Recently, the issue of remote dynamics emerged in complex network systems is an amazing and intriguing topic and receives great attention, among which the remote synchronization has attracted the most attention [26–33]. Remote synchronization is a nonlocal coordination state that describes the synchrony phenomenon among two subpopulations that are indirectly coupled to each other. As the remote synchronization was termed by Bergner *et al.* [27], lots of contributions were achieved in this field. For example, Punetha *et al.* discovered the delay-induced remote synchronization in bipartite networks of phase oscillators [29]. Kumar and Rosenblum exposed the two mechanisms of remote synchronization in a chain of Stuart-Landau oscillators [31]. Yang *et al.* unveiled the phase frustration induced remote synchronization [33].

Besides the remote synchronization, other topics relating to the manifestations of remote dynamics are investigated and reported, which are significant in revealing the mechanisms of a variety of behaviors occurring in miscellaneous systems. Ruzzene *et al.* studied the remote pacemaker control of chimera states in multilayer networks of neurons [34]. Liu and coworkers reported the remote signal propagation in the specific biological network models consisting of bistable oscillators and Hindmarsh-Rose neurons [35,36]. However,

*Contact author: qianyu0272@163.com
†Contact author: leizhao1010@163.com
‡Contact author: zgzheng@hqu.edu.cn

very little attention has been paid to the remote dynamics on the paced excitable complex systems. It is well known that the paced excitable complex network is a paradigmatically theoretical platform to study the response dynamics of brain systems with external stimulations and reveal the mechanisms of the corresponding brain functions. A traditional viewpoint is that the excitable pacing signal should propagate from the source to its excited neighbors in a sequential rule, which is known as the normal *sequential response mode* (SRM). It is significant to study the availability and mechanism of remote response dynamics emerged on paced excitable systems.

To explore this issue, in the present paper, the *C. elegans* network, which has been widely applied to study the collective behaviors in neural systems, is adopted as the substrate to construct a specific excitable complex system. By extensively exploring the response modes emerged on the *paced excitable C. elegans network* (PECN), we found that, besides the normal SRM, a response mode that breaks the sequence rule and contains isolated excited clusters or even isolated excited nodes on the propagation path of the response structure can be detected. Such remote response nodes and clusters are excited discontinuously from the source node, forming the phenomenon of the *remote response mode* (RRM).

The remainder of the paper is organized as follows. Section II introduces the working model of the PECN. The SRM and the RRM that can self-organize to emerge on the PECN are investigated in Sec. III, respectively. In Sec. IV, an *effective-driving analysis approach* (EDAA) is proposed to discuss the mechanism for the emergence of the RRM. The applicability and the universality of the EDAA are explored in Sec. V. Finally, we give the conclusion in the last section.

II. THE PACED EXCITABLE *C. ELEGANS* NETWORK MODEL

As our working substrate, the typical topology of the *C. elegans* network is displayed in Fig. 1(a), which consists of 277 nodes (shown by red dots) and 2105 directional links (black lines) [37]. It is revealed clearly in Fig. 1(a) that both the spatial and degree distribution of the cells on *C. elegans* network are heterogeneous. Figure 1(b) presents the corresponding adjacent matrix A of the *C. elegans* network, where each yellow dot corresponding to the matrix element $A_{i,j}$ represents a directional link from node j to node i. Since $A_{i,j} \neq A_{j,i}$ for many i and j, the adjacent matrix is asymmetric, implying the heterogeneity of the real *C. elegans* network.

Based on the substrate adopted by the *C. elegans* network, the classical Bär-Eiswirth model [38] is utilized as the representative local dynamics to construct the excitable *C. elegans* network. Furthermore, a periodic pacing is applied on a specific source node to probe the response modes emerged on the system. The PECN model considered in the present paper is governed by the following equations:

$$\frac{du_i}{dt} = \frac{1}{\varepsilon}u_i(1-u_i)\left(u_i - \frac{v_i+b}{a}\right) + D\sum_{j=1}^{N} A_{i,j}(u_j - u_i) + \delta_{i,S}A\sin(2\pi f t), \tag{1}$$

$$\frac{dv_i}{dt} = f(u_i) - v_i. \tag{2}$$

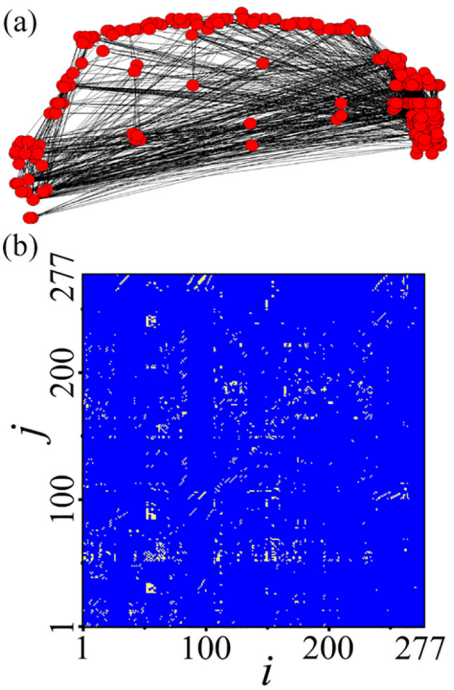

FIG. 1. (a) The structure of the *C. elegans* network, which consists of 277 nodes (red dots) and 2105 directional links (black lines). (b) The corresponding adjacent matrix A of the *C. elegans* network, where the yellow dot located at matrix element $A_{i,j}$ indicates that there exists a directional link from the elements j to i.

In the above two equations, the subscripts i, j $(i, j = 1, 2, \ldots, N)$ label the nodes on the network, where the size of the *C. elegans* system is $N = 277$. Here u and v are respectively the activation and the recovery variables of the local excitable cell, which can present the membrane potential and the recovery current in the case of imitating neural dynamics. Constants a, b, and ε are the three dimensionless characteristic parameters that can effectively regulate the local excitable dynamics, among which parameters a and b determine the excitation threshold and ε modulates the time scale of the two variables. The function $f(u)$ is piecewise and obeys the form $f(u) = 0$ for $u < \frac{1}{3}$, $f(u) = 1 - 6.75u(u-1)^2$ for $\frac{1}{3} \leqslant u \leqslant 1$, and $f(u) = 1$ for $u > 1$.

The interplays among the nodes on the network are realized by the diffusive coupling term $D\sum_{j=1}^{N} A_{i,j}(u_j - u_i)$, where D is the coupling strength determining the interaction intensity between linking elements. $A_{i,j}$ represents the adjacency matrix element, which is defined as $A_{i,j} = 1$ if there is a directional link from the nodes j to i, and $A_{i,j} = 0$ otherwise. A periodic pacing $A\sin(2\pi f t)$ is adopted and is applied on the source node S via introducing the Kronecker function $\delta_{i,S}$, i.e., $\delta_{i,S} = 1$ for $i = S$ and $\delta_{i,S} = 0$ for $i \neq S$. The control parameters A and f are respectively the amplitude and the frequency of the external periodic pacing. In the following, Eqs. (1) and (2) are integrated by the forward Euler integration algorithm with the time step $\Delta t = 0.02$. The system parameters are fixed as $a = 0.84$, $b = 0.07$, $\varepsilon = 0.04$, and $D = 1.0$. The homogeneous rest state, i.e., $[u_i(t=0), v_i(t=0)] = (0, 0)$ $(i = 1, 2, \ldots, N)$, is adopted as the initial condition in numerical simulations.

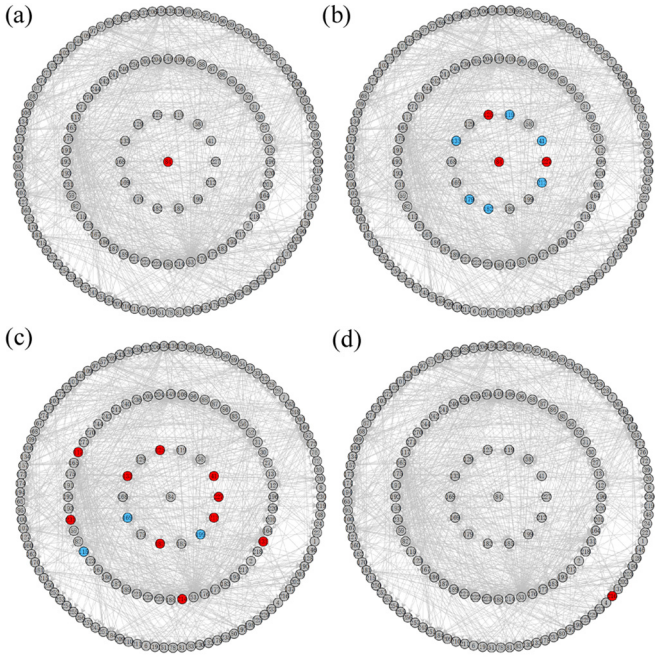

FIG. 2. The response patterns on the PECN obtained at $t = 401.4$ (a), 401.8 (b), 402.8 (c), and 403.8 (d). The periodic pacing $A\sin(2\pi ft)$ with $(A, f) = (1.8, 0.1)$ is adopted and applied on the source node $S = 84$. The elements are sequenced from the central source node to the outside according to the directional connections. The states of each node are divided into three categories, i.e., the rest state ($u < 0.2$), the exciting state ($0.2 \leqslant u < 0.5$), and the excited state ($u \geqslant 0.5$), which are colored in gray, blue, and red, respectively. Here $u_c = 0.5$ is utilized as the excitation threshold to judge whether the node in the network is excited or not.

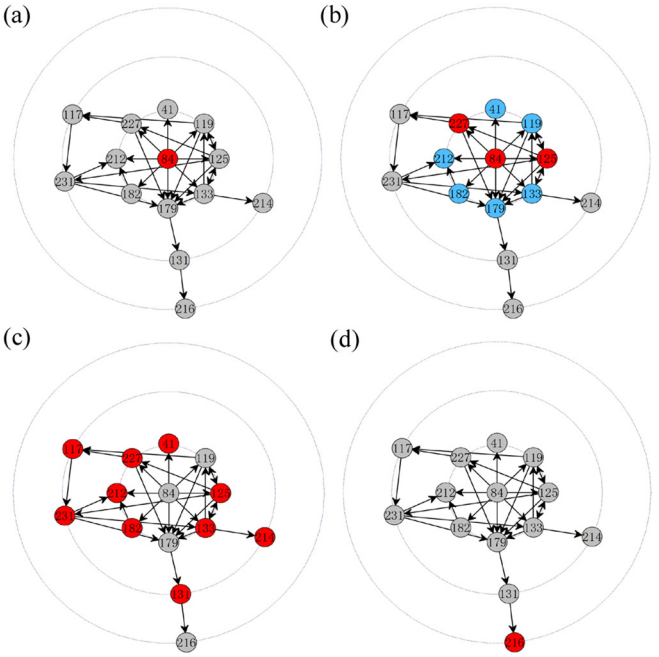

FIG. 3. The response structures of Fig. 2 by discarding the nonexcited nodes, by which the normal SRM is identified.

III. THE SEQUENTIAL RESPONSE MODE AND THE REMOTE RESPONSE MODE

In this part, we mainly focus on the response mode that can self-organize to emerge on the PECN. The periodic pacing $A\sin(2\pi ft)$ with $(A, f) = (1.8, 0.1)$ is first tested and applied on the source node $S = 84$. The corresponding response patterns obtained at four different instants are displayed in Figs. 2(a)–2(d), respectively. Here we should mention that the elements in these pictures are sequenced from the central source node to the outside according to the directional connections. Furthermore, the states of each node are divided into three categories, i.e., the rest state ($u < 0.2$), the exciting state ($0.2 \leqslant u < 0.5$), and the excited state ($u \geqslant 0.5$), which are colored in gray, blue, and red, respectively, and $u_c = 0.5$ is utilized as the excitation threshold to judge whether a node in the network is excited or not.

Figure 2 gives a typical example that the pacing signal propagates sequentially from the source node located in the innermost layer to the nodes seated in the outside layers. We call this response mode as the normal SRM. To determine the propagations of an arbitrary SRM, a reduction scheme can be proposed to obtain the reduced response structure by discarding the nonexcited nodes, i.e., by deleting the nodes i $(i = 1, 2, \ldots, N)$ with $\mathrm{Max}\{u_i(t)\} < u_c$. Here $\mathrm{Max}\{u_i(t)\}$ indicates the maximum value of the time series $u_i(t)$. This means that only the excited nodes will be reserved in the response structure. By using this scheme, the corresponding response structures of Figs. 2(a)–2(d) are obtained and revealed in Figs. 3(a)–3(d), respectively. It is shown clearly that the excitable waves presented in Fig. 2 do propagate with a sequence from the inner paced source node $S = 84$ to its outside neighbors and then to the neighbors' outsiders and so on. Importantly, each node in the response structure at least has an excited upstream driving neighbor, which can kick it from the rest state to exceed the excitation threshold and make it become an excited node. Therefore the response structures exposed in Fig. 3 imply a normal SRM on the PECN.

However, besides the normal SRM, it is important to explore other kinds of response modes that can self-organize to emerge on the PECN. To this end, different source nodes are tested. An example obtained at the pacing parameters $(A, f) = (1.8, 0.1)$ and the source node $S = 126$ is obtained, which is presented in Fig. 4. It can be found from the four response patterns at different moments in Figs. 4(a)–4(d) that the pacing signal can still propagate sequentially from the inner source node to the outside nodes, which is similar to the response mode revealed in Fig. 2. It seems that the response mode revealed in Fig. 4 is also a normal SRM.

To further testify whether the above judgment is true, similar reduced response topologies to Fig. 4 are obtained by discarding the nonexcited nodes, which are shown in Figs. 5(a)–5(d), respectively. Surprisingly, beyond our expectations, besides the above normal sequential response cluster located at the lower right corner, i.e., the excited cluster (126, 140, 141, 161, 162, 163), which is triggered sequentially from the inner paced source node to the outsiders, some isolated excited clusters such as the cluster (100, 29, 266) and the isolated excited nodes (252), (253), (254), (255), (256), (257), and (269) have also been observed in the response structures.

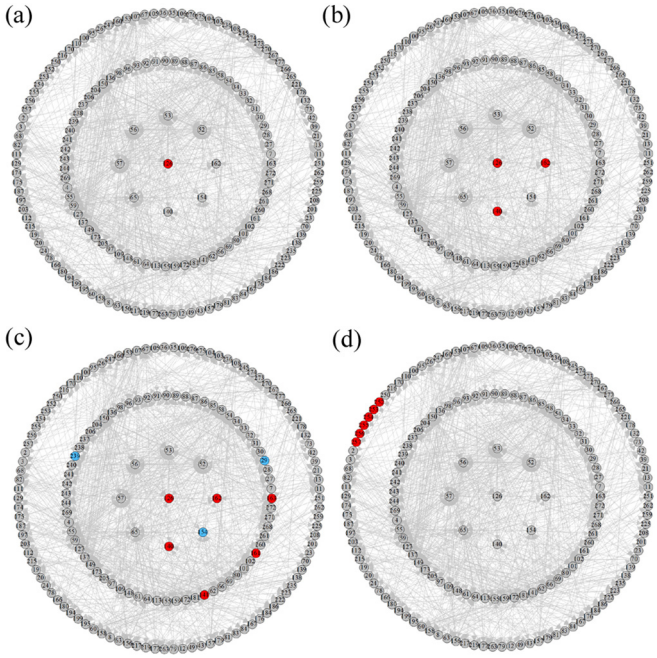

FIG. 4. The similar response patterns with another pacing parameter combination $(A, f) = (1.8, 0.1)$ and source node $S = 126$. The states are obtained at $t = 401.6$ (a), 402.4 (b), 403.4 (c), and 405.6 (d).

Let us further analyze the above two types of special cases. It is shown in Fig. 5 that, for the isolated excited cluster (100, 29, 266), the node 100 is the upstream node and can be considered as the "source node," whose firings may agitate the two downstream nodes 29 and 266. However, no excited upstream driving nodes are found to offer stimulations to

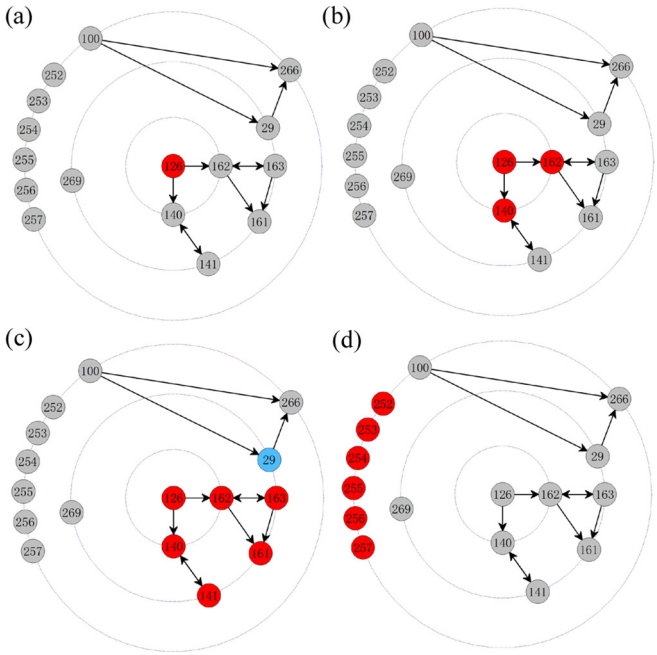

FIG. 5. The similar response structures of Fig. 4, by which the RRM is confirmed.

impulse this fake "source node." Similar phenomena also happen to those isolated excited nodes, which are triggered without other excited upstream driving neighbors. This surprising phenomenon is distinctly contrary to the normal point of view on a sequential propagation that the excitable pacing signal should propagate from the source to its excited neighbors and then to the neighbors' excited neighbors and so on. This means that each node located in the propagation path should have an excited upstream driving neighbor. Otherwise, the excitable wave will damp and the propagation will terminate if there exists a nonexcited node in the propagation path. Therefore the response mode exposed in Fig. 5 is distinctly different from the normal SRM. As for the existence of the nodes without any excited upstream driving neighbors, such as the above isolated nodes and fake "source node" in the response structures, which are excited discontinuously from the source node, we call these two types of special excited elements as the remote response nodes, and consequently this response mode is named as the RRM.

IV. THE MECHANISM DISCUSSION BASED ON THE EFFECTIVE-DRIVING ANALYSIS APPROACH

It is inspiring to seek for the mechanism of the RRM emerged on the PECN. The remote response node 257 shown in the response structures of Fig. 5 is utilized as the example to explore this issue, and the excitable wave propagation paths from the source node to this isolated excited node are revealed in Fig. 6(a). The pink, green, purple, and orange circles respectively represent the excited remote response node 257 (i.e., the target node in the current case), the nonexcited upstream driving neighbors of the target node, the source node $S = 126$, and the excited intermediate elements between the source node and the two nonexcited nodes. The typical time series of these four different types of nodes are also presented, in which the black and gray dashed lines denote the rest state and the excitation threshold $u_c = 0.5$, respectively.

It is shown in Fig. 6(a) that, for the first two rounds of excitations, the excitable waves can propagate sequentially from the purple source node to the orange excited intermediate elements. However, as the excitable waves propagate to the two green nodes 149 and 150 (i.e., the two upstream driving neighbors of the remote response node 257), the normal suprathreshold excitations terminate, instead of which these two green nodes perform subthreshold vibrations. More surprisingly, with the stimulations from these two subthreshold vibration neighbors, the pink target node 257 can execute a normal suprathreshold excitation again. This discontinuous propagation process can explicitly make the pink target node 257 become the remote response node in the response structures, and the RRM can be definitely identified on the PECN.

A normal viewpoint is that more upstream drivings on an excitable node implies an easier excitation. Nevertheless, a contrary observation of the excitable wave propagation paths in Fig. 6(a) shows that both nonexcited nodes 149 and 150 (green) have more incoming upstream drivings (four for node 149 and three for 150) than the pink excited remote response node (it only has two). It is thus fundamental to explore the reason why the remote response node receiving only two upstream drivings can execute normal suprathreshold excitation,

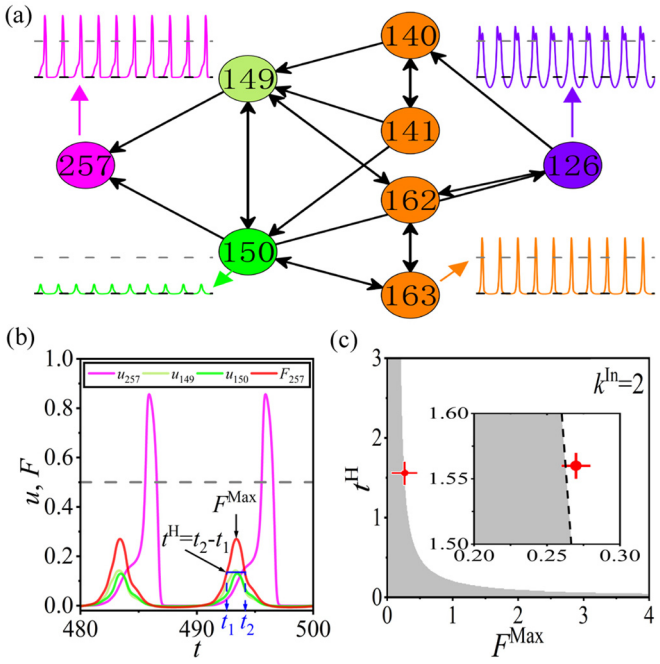

FIG. 6. (a) The mechanism analysis of the RRM. The pink, green, purple, and orange nodes are respectively the excited remote response node (i.e., the target node in this case), the nonexcited upstream driving neighbors of the target node, the source node, and the excited intermediate elements between the source node and the two nonexcited nodes. The typical time series of these four different types of nodes are also presented, in which the black and gray dashed lines denote the rest state and the excitation threshold $u_c = 0.5$, respectively. (b) The time series of the excited target node 257 and its two nonexcited upstream driving neighbors 149 and 150. Here F_{257} implies the equivalent resultant drive of the target node, which comes from the corresponding upstream driving neighbors. In the current case, $F_{257} = u_{149} + u_{150}$. (c) The phase diagram on the $(F^{\mathrm{Max}}, t^{\mathrm{H}})$ plane for an arbitrary target node with $k^{\mathrm{In}} = 2$, which reveals two distinct parameter domains, i.e., the white excited region and the gray nonexcited region. The red cross represents the equivalent resultant drive received by the excited remote response node 257 in the current case, which locates in the white excited region. The inset shows the corresponding local amplification.

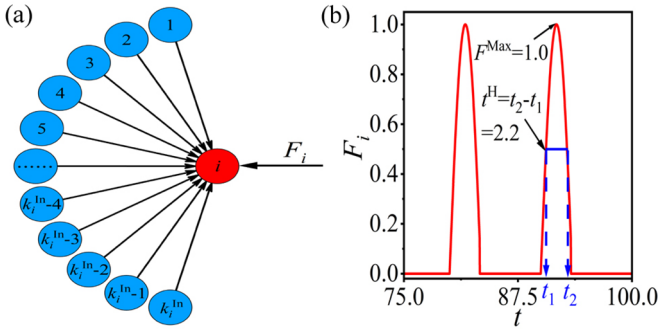

FIG. 7. (a) The schematic diagram of the EDAA. Here the red node i represents an arbitrary target node needed to judge whether it can be excited or not in the RRM. It has k_i^{In} incoming upstream neighbors, which are denoted by blue nodes and labeled from 1 to k_i^{In}. F_i indicates the equivalent resultant drive acting on the target node i received from all of its k_i^{In} upstream driving neighbors. (b) An example of the equivalent resultant drive F_i with two characteristic quantities $F^{\mathrm{Max}} = 1.0$ and $t^{\mathrm{H}} = 2.2$. Here F^{Max} and t^{H} are respectively the maximum value of F_i and the duration when $F_i \geqslant \frac{1}{2}F^{\mathrm{Max}}$ in a period, by which the equivalent drive function can be uniquely determined.

while the two green upstream driving neighbors gaining more cannot. This should be the mechanism in forming the RRM on the PECN, which is the main task we aim to explore.

It is inspiring to propose an EDAA to answer the above questions. A schematic diagram of the EDAA is illustrated in Fig. 7(a), where an arbitrary target node i (red circle, i.e., the node needed to judge whether it can be excited or not in the RRM) has k_i^{In} incoming upstream neighbors (blue circles) and the accumulative drivings received from all of its k_i^{In} upstream neighbors in real cases are considered as an equivalent resultant drive, which is denoted by a time-dependent function F_i. The dynamical equations of this target node can be written as

$$\frac{du_i}{dt} = \frac{1}{\varepsilon}u_i(1-u_i)\left(u_i - \frac{v_i+b}{a}\right) + D\left(F_i - k_i^{\mathrm{In}}u_i\right), \tag{3}$$

$$\frac{dv_i}{dt} = f(u_i) - v_i. \tag{4}$$

The key point of the EDAA can be understood as follows. Suppose an arbitrary target node receives an equivalent resultant drive from all of its incoming upstream neighbors, which may drastically change its dynamical behavior. Only when the equivalent resultant drive surpasses a critical value, this target node can be excited. This indicates that a critical threshold of the equivalent resultant drive is the crucial point to judge whether a target node can be excited or not. Based on the above reduced model, one can conveniently unfold this issue by effectively working out the necessary condition for the excitation of an arbitrary target node in the RRM according to the equivalent resultant drive. The most important merit of the present EDAA is that this approach is irrelevant of network topology and applicable to various types of cases.

Enlightened by the features of the equivalent resultant drives received by the target nodes in the PECN, we empirically construct the following time-dependent function F_i to mimic the equivalent resultant drive on the ith target node as

$$F_i = \begin{cases} F^{\mathrm{Max}}\sin\left[\frac{2\pi}{3t^H}(t - JT_s)\right] & JT_s \leqslant t \leqslant \frac{3}{2}t^H + JT_s \ (J = 1, 2, 3, \ldots), \\ 0 & \text{else.} \end{cases} \tag{5}$$

In Eq. (5), T_s is the period of the equivalent driving function F_i, which is determined by the frequency of the external periodic pacing as $T_s = \frac{1}{f}$. F^{Max} and t^{H} are respectively the maximum value of F_i and the duration when $F_i \geqslant \frac{1}{2}F^{\mathrm{Max}}$ in one period. These two key control parameters uniquely determine the form of function F_i, based on which diverse equivalent

resultant drives received by an arbitrary target node i in real cases can be effectively mimicked. Figure 7(b) presents the time series of an equivalent resultant drive F_i for $F^{\mathrm{Max}} = 1.0$, $t^{\mathrm{H}} = 2.2$, and $f = 0.1$. In the following we will focus on how the two vital control parameters (i.e., F^{Max} and t^{H}) impact the excitation of the given target node and expose the corresponding excitable parameter combinations.

Let us first apply the EDAA to analyze why the pink remote response node 257 with only two incoming upstream drivings shown in Fig. 6(a) can be excited. Figure 6(b) presents the time series of the node 257 with the pink curve and its two nonexcited upstream driving neighbors 149 and 150 with the two green curves. It is shown explicitly that, with the stimulations from these two subthreshold vibration neighbors, the target node 257 can definitely execute a normal suprathreshold excitation. To explain this counterintuitive phenomenon, the equivalent resultant drive of the target node in the current case is obtained easily as $F_{257} = u_{149} + u_{150}$, which is revealed by the red curve. Moveover, the two corresponding characteristic parameters F^{Max} and t^{H} are also labeled.

To explain why the target node 257 with only two incoming upstream drivings can be excited under the equivalent resultant drive possessing the above two characteristic parameters, the phase diagram on the $(F^{\mathrm{Max}}, t^{\mathrm{H}})$ plane for an arbitrary target node with $k^{\mathrm{In}} = 2$ is computed according to the EDAA, as explicitly exposed in Fig. 6(c). The local amplification shown in the inset reveals clearly that there exist two distinct parameter domains. The white regions denote the parameter regime where the target node can be excited, and the gray region corresponds to the regime where the target node fails to be excited. It can be clearly seen that the parameter combination $(F^{\mathrm{Max}}, t^{\mathrm{H}})$ for the target node 257 labeled as the red cross is located in the white excited region. This strongly confirms that the target node can execute a normal suprathreshold excitation although its two upstream neighbors perform subthreshold vibrations, which forms the RRM on the PECN.

It is also necessary to answer the question why the two upstream neighbors of the remote response node cannot carry out normal suprathreshold excitations (i.e., the key point in forming the RRM) even if they have more incoming upstream drivings. We choose the nonexcited upstream driving neighbor 150 as the target node to explore this issue. Figure 8(a) displays the local network structure of the target node 150, which has two incoming excited upstream neighbors (orange circles) and 24 incoming nonexcited upstream neighbors (gray ones). To apply the EDAA, the time series of the target node 150 and its equivalent resultant drive $F_{150} = \sum_{i=1}^{k_{\mathrm{in}}=26} u_i$ ($i \in$ upstream neighbors) are plotted in Fig. 8(b), where the two corresponding characteristic parameters F^{Max} and t^{H} are also denoted.

To verify whether a target node under the equivalent resultant drive can be excited, the phase diagram on the $(F^{\mathrm{Max}}, t^{\mathrm{H}})$ plane for an arbitrary target node with $k^{\mathrm{In}} = 26$ is plotted in Fig. 8(c), where similar white excited region and gray nonexcited region to Fig. 6(c) are obtained. The red cross located in the gray nonexcited region represents the equivalent resultant drive received by the above nonexcited target node 150. This further confirms the nonexcited state of the target node, which plays a key role in forming the RRM.

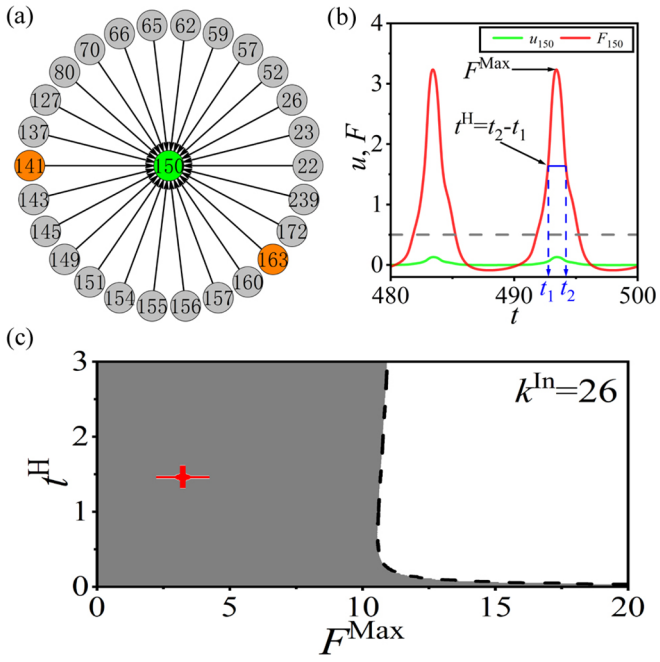

FIG. 8. The mechanism analysis of the nonexcited node in the RRM. Here node 150, i.e., the nonexcited upstream driving neighbor of the excited remote response node 257, is utilized as the target node to explore this issue. (a) The local network structure of the target node 150, which has two incoming excited upstream neighbors (orange circles) and 24 incoming nonexcited upstream neighbors (gray ones). (b) The time series of the target node 150 and its equivalent resultant drive F_{150} (here $F_{150} = \sum_{i=1}^{k_{\mathrm{in}}=26} u_i$, $i \in$ upstream neighbors). (c) The phase diagram on the $(F^{\mathrm{Max}}, t^{\mathrm{H}})$ plane for an arbitrary target node with $k^{\mathrm{In}} = 26$. The red cross represents the equivalent resultant drive received by the nonexcited target node 150 in the current case, which locates in the gray nonexcited region.

Furthermore, by comparing the phase diagrams respectively shown in Figs. 6(c) and 8(c) one can find that the number of incoming upstream neighbors of the target node k^{In} is a key factor in determining the excitability of the given node. It is revealed explicitly that the larger the k^{In} is, the smaller the white excited region is. This means that the more incoming upstream neighbors an excitable node has, the harder it can be excited. Therefore, based on the EDAA, the mechanism of the RRM emerged on the PECN can be well explained.

V. THE APPLICABILITY AND THE UNIVERSALITY OF THE EFFECTIVE-DRIVING ANALYSIS APPROACH

The above discussions indicate that remote response nodes can self-organize to emerge on paced networks. This is the key point for the formation of the RRM. The emergence of remote response nodes should meet the following necessary conditions.

(i) All upstream driving neighbors of remote response nodes are nonexcited.

(ii) With the stimulations from these nonexcited upstream neighbors, remote response nodes must be excited.

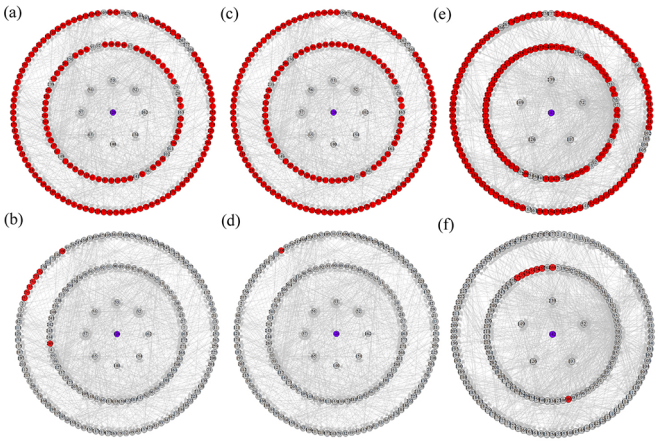

FIG. 9. Identifying the RRM on the PECN via the EDAA. (a, c, e) The patterns (red nodes) after the first operation process (i.e., by selecting the nodes only possessing nonexcited upstream driving neighbors). (b, d, f) The remote response nodes (red nodes) after the second operation process (i.e., by exploiting the EDAA on the patterns shown in the first row). The central purple node in each panel denotes the source node on which the external periodic pacing is applied. The pacing parameters and source node are selected as $(A, f) = (1.8, 0.1)$ and $S = 126$ for (a) and (b) (left column), $(A, f) = (2.7, 0.2)$ and $S = 126$ for (c) and (d) (middle column), and $(A, f) = (1.0, 0.1)$ and $S = 142$ for (e) and (f) (right column).

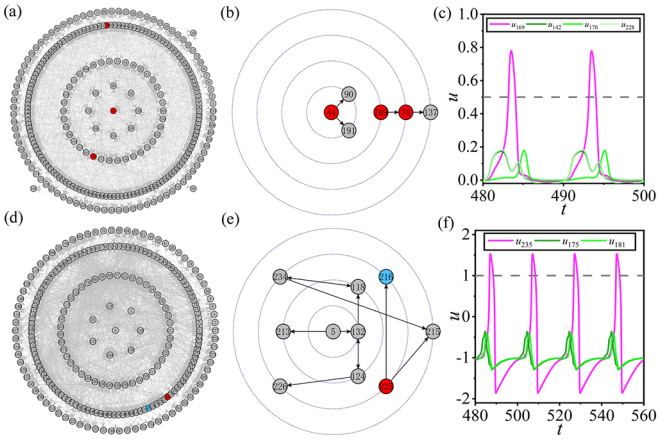

FIG. 10. (a–c) A RRM emerged on a directional Erdös-Rényi random network consisting of excitable Bär-Eiswirth elements. The pacing combination $(A, f) = (3.44, 0.1)$ and source node $S = 44$ are utilized here. (a) The response pattern obtained at instant $t = 413.9$. (b) The corresponding response structure of the RRM. (c) The time series of the remote response node u_{169} and its upstream driving neighbors. (d–f) The similar RRM emerged on the paced *C. elegans* network containing paradigmatic excitable FHN cells. The pacing combination $(A, f) = (1.5, 0.05)$ and source node $S = 5$ are adopted here. (d) The response pattern obtained at instant $t = 408.4$. (e) The similar response structure. (f) The time series of the remote response node u_{235} and its upstream driving neighbors.

It is thus valuable to design an algorithm to search and identify the RRM on the PECN by utilizing the EDAA. According to the above two essential requirements, the following operation procedure is proposed to identify the RRM.

(i) Select the nodes with only nonexcited upstream driving neighbors.

(ii) Apply the EDAA to the nodes selected in the first step to choose the excited ones.

By implementing the above two operational steps, the remote response nodes can be picked out precisely without knowing the state information of these nodes, and the RRM can be identified on the PECN.

One adopts the RRM presented in Figs. 4 and 5 [i.e., the pacing parameters and source node are $(A, f) = (1.8, 0.1)$ and $S = 126$] as the example to test our method. Figure 9(a) unveils the pattern after the first operation step. It is clearly shown that, by selecting the nodes only possessing nonexcited upstream driving neighbors, lots of elements satisfying this necessary condition are picked out (red nodes), which are considered as the candidates for step 2. Now we can perform step 2 by exploiting the EDAA on the pattern displayed in Fig. 9(a), and the corresponding result is revealed in Fig. 9(b), where the left red cells are the remote response nodes filtered according to our method. By comparing with the response structures exposed in Fig. 5, only the isolated excited nodes and the excited fake "source node" are all identified exactly, based on which the emergence of RRM can be confirmed on the PECN.

Let us further verify the universality of the EDAA. We first test this for other pacing parameters. Figures 9(c) and 9(d) (middle column in Fig. 9) reveal the results obtained for a pacing $(A, f) = (2.7, 0.2)$. The source node is also fixed as the case shown in Figs. 9(a) and 9(b) (left column in Fig. 9). By applying our approach, only one remote response node is filtered, based on which the RRM can be expected on the PECN with current pacing. More importantly, this prediction is confirmed in our numerical simulations (not shown here). Now we check the method for other source nodes, on which the external periodic pacing is applied. The right column in Fig. 9 [i.e., Figs. 9(e) and 9(f)] shows the remote response nodes for $(A, f) = (2.7, 0.2)$ and $S = 126$ (both pacing parameter combination and response node are changed), which coincide with the experimental data very well (also not shown here). All the results presented in Fig. 9 can definitely confirm the applicability and the universality of our method in identifying the RRM on the PECN, especially the EDAA we propose in the present paper.

VI. THE ROBUSTNESS OF THE RRM EMERGED ON PACED EXCITABLE COMPLEX NETWORK SYSTEMS

To verify the robustness of the RRM emerged on paced excitable complex network systems, a directional classical network model is first tested. Figures 10(a)–10(c) show a RRM emerged on a directional excitable Erdös-Rényi random network, which is constructed with system size $N = 277$ and connection probability $p = 0.02$. The Bär-Eiswirth model is adopted as the local dynamics, and the system parameters are selected as the above figures. The pacing combination $(A, f) = (3.44, 0.1)$ and source node $S = 44$ are utilized. Here we should mention that, based on the above network structure parameters (i.e., $N = 277$ and $p = 0.02$), the total number of the directional edges in the network is expected to be $pN(N-1) \approx 1529$, which is close to the number of

directional links of the *C. elegans* network. This may make the constructed directional excitable Erdös-Rényi random networks have similar structural properties to observe the RRMs. Furthermore, we have also confirmed in numerical simulations that the combination of the above structure parameters and system parameters is more beneficial for the emergence of the RRMs on paced directional excitable Erdös-Rényi random networks.

Figure 10(a) displays the response pattern obtained at instant $t = 413.9$. The corresponding response structure is exposed in Fig. 10(b), by which the remote response node 169 is exposed. Figure 10(c) presents the time series of the remote response node u_{169} (shown by the pink curve) and its three nonexcited upstream driving neighbors (denoted by the green curves). Based on the results revealed in Figs. 10(a)–10(c) we can conclude that the RRM can also self-organize to emerge on other paced directional excitable complex networks.

Local dynamics also needs to be discussed to check the robustness of the RRM emerged on paced excitable complex network systems. Here the following paradigmatic excitable FitzHugh-Nagumo (FHN) cell is adopted as the local dynamics:

$$\frac{du_i}{dt} = \frac{1}{\varepsilon}\left(u_i - \frac{u_i^3}{3} - v_i\right) + D\sum_{j=1}^{N} A_{i,j}(u_j - u_i) + \delta_{i,S} A \sin(2\pi f t), \tag{6}$$

$$\frac{dv_i}{dt} = \varepsilon(u_i + \beta - \gamma v_i). \tag{7}$$

The system parameters are selected as $\varepsilon = 0.2$, $\beta = 0.7$, $\gamma = 0.5$, and $D = 0.5$. The *C. elegans* network is used as the substrate, and the pacing parameter combination $(A, f) = (1.5, 0.05)$ and source node $S = 5$ are utilized here. The corresponding results are displayed in Figs. 10(d)–10(f), where the response pattern obtained at instant $t = 408.4$ [Fig. 10(d)], the similar response structure [Fig. 10(e)], and the time series of the remote response node u_{235} [the pink curve in Fig. 10(f)] and its upstream driving neighbors [the two green curves in Fig. 10(f)] are respectively presented. Here we should mention that, based on the excitation features of the local FHN cell [see the pink curve in Fig. 10(f)], the states of each element are classified into three categories according to the following standards, i.e., the rest state ($u < 0$, colored in gray), the exciting state ($0 \leqslant u < 1$, blue), and the excited state ($u \geqslant 1$, red). So $u_c = 1$ is adopted as the excitation threshold to judge whether each cell in the network is excited or not. It is shown that the RRM can also self-organize to emerge on the paced excitable *C. elegans* network with other local dynamics. All these results revealed in Fig. 10 can definitely confirm that the RRM emerged on paced excitable complex network systems is robust.

Besides the 1:1 RRMs exposed in the above sections, the RRMs with other drive-response frequency ratios can also be observed. Figure 11 presents three examples of the RRMs with drive-response frequency ratios 2:1 [first row, $(A, f) = (0.5, 0.1)$ and $S = 124$], 3:1 [second row, $(A, f) = (1.2, 0.1)$ and $S = 228$], and 4:1 [third row, $(A, f) = (1.0, 0.1)$ and $S = 132$] emerged on the paced *C. elegans* network consisting of paradigmatic excitable FHN cells. The left, middle, and right columns are respectively the response patterns obtained at instants $t = 415.1$ [Fig. 11(a)], $t = 466.5$ [Fig. 11(d)], and $t = 497.18$ [Fig. 11(g)]; the corresponding response structures of the RRMs [Figs. 11(b), 11(e), and 11(h)]; and the time series of the remote response nodes u_{235} [Fig. 11(c)], u_{232} [Fig. 11(f)], and u_{235} [Fig. 11(i)] and their upstream driving neighbors. These results further confirm the existence of the complicated RRMs on paced excitable complex network systems. This is one of the most important attributes of the excitable response dynamics, which can give us clues in understanding the complex response modes of brain systems under external stimuli.

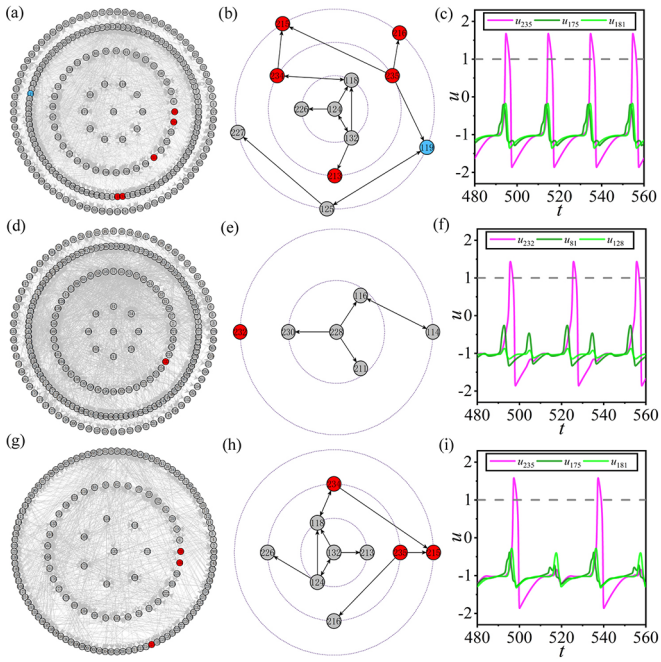

FIG. 11. The RRMs with drive-response frequency ratios 2:1 [first row, $(A, f) = (0.5, 0.1)$ and $S = 124$], 3:1 [second row, $(A, f) = (1.2, 0.1)$ and $S = 228$], and 4:1 [third row, $(A, f) = (1.0, 0.1)$ and $S = 132$] emerged on the paced *C. elegans* network consisting of paradigmatic excitable FHN cells. (a, d, g) The response patterns obtained at instants $t = 415.1$ (a), $t = 466.5$ (d), and $t = 497.18$ (g). (b, e, h) The corresponding response structures of the RRMs. (c, f, i) The time series of the remote response nodes u_{235} (c), u_{232} (f), and u_{235} (i) and their upstream driving neighbors.

VII. CONCLUSION AND DISCUSSION

In conclusion, various response modes emerged on the PECN are extensively explored. By applying the external periodic pacing on the specific source node with certain pacing parameter combinations, the normal sequential response mode is usually observed, in which the excitable waves can propagate sequentially from the inner paced source node to its outside neighbors and then to the neighbors' outsiders and so on. However, by altering source nodes and pacing parameters, a remote response mode is detected. Without any excited upstream driving neighbors in the response structures, these RRMs manifest as the existence of some isolated excited clusters and even isolated excited nodes, besides the normal

sequential response clusters. The existence of such remote response nodes, which are excited discontinuously from the source node, forms the phenomenon of RRM.

The mechanism of the RRMs emerged on the PECN is analyzed in detail. An effective-driving analysis approach is proposed. The effective topology is composed of an arbitrary target node possessing k^{In} incoming upstream driving neighbors. The target node is acted on by an equivalent resultant drive received from all of its upstream neighbors. By utilizing the EDAA for each target node in the network, one can precisely predict whether it can be excited or not without knowing any of its state information. The EDAA analysis highlights the significance of the excited nodes possessing nonexcited upstream driving neighbors, which is confirmed as the key factor in forming the RRM on the PECN.

The applicability and the universality of the EDAA are further verified. We have demonstrated that our method can be applied to identify the RRMs on the PECN with diverse source nodes and various pacing parameter combinations. The RRM and the EDAA proposed in this paper should also be applicable to general excitable systems. Furthermore, both the robustness of the RRM phenomena with respect to network structure and local dynamics are discussed in detail. It is found that the RRM emerged on paced excitable complex network systems is robust. Moreover, the RRMs with other drive-response frequency ratios can also be observed. This further confirms the existence of the complicated RRMs on paced excitable complex network systems.

The issue of response dynamics that can self-organize to emerge on paced excitable systems is one of the most important topics in the fields of nonlinear science and network science. A response mode, i.e., the RRM, that breaks the sequence rule and contains isolated excited clusters or even isolated excited nodes on the propagation path of the response structure is revealed. Furthermore, besides the normal 1:1 RRMs, RRMs with other drive-response frequency ratios (such as the 2:1, 3:1, and 4:1 RRMs) are also exposed. This is the most typical attribute of the excitable response dynamics, which may not be observed for other local dynamics. Importantly, a universal theoretical analysis method is proposed to identify the RRMs on general paced excitable complex network systems. These findings are not revealed in previous works [35,36]. We think our contributions presented in this paper can give us clues in understanding the complex response modes of brain systems under external stimuli and will have great impacts in related fields.

ACKNOWLEDGMENTS

This work is supported by the National Natural Science Foundation of China (Grants No. 12375033 and No. 12375031), the Natural Science Basic Research Plan in Shaanxi Province of China (Grants No. 2022JZ-03, No. 2022GD-TSLD-27, and No. 2024SF-YBXM-134), the Shaanxi Fundamental Science Research Project for Mathematics and Physics (Grants No. 22JSY021 and No. 23JSQ051), the Baoji University of Arts and Sciences Innovative Research Project of Postgraduates (Grants No. YJSCX23YB34 and No. YJSCX22ZD02), and the Youth Innovation Team of Shaanxi Universities.

[1] D. J. Watts and S. H. Strogatz, Collective dynamics of "small-world" networks, Nature (London) **393**, 440 (1998).

[2] A.-L. Barabási and R. Albert, Emergence of scaling in random networks, Science **286**, 509 (1999).

[3] A. Arenas, A. Díaz-Guilera, J. Kurths, Y. Morenob, and C. Zhoug, Synchronization in complex networks, Phys. Rep. **469**, 93 (2008).

[4] X. Zhang, S. Boccaletti, S. Guan, and Z. Liu, Explosive synchronization in adaptive and multilayer networks, Phys. Rev. Lett. **114**, 038701 (2015).

[5] S. Boccaletti, J. A. Almendral, S. Guana, I. Leyva, Z. Liu, I. Sendiña-Nadal, Z. Wang, and Y. Zou, Explosive transitions in complex networks' structure and dynamics: Percolation and synchronization, Phys. Rep. **660**, 1 (2016).

[6] E. Rybalova, G. Strelkova, E. Schöll, and V. Anishchenko, Relay and complete synchronization in heterogeneous multiplex networks of chaotic maps, Chaos **30**, 061104 (2020).

[7] A. Roxin, H. Riecke, and S. A. Solla, Self-sustained activity in a small-world network of excitable neurons, Phys. Rev. Lett. **92**, 198101 (2004).

[8] S. Sinha, J. Saramäki, and K. Kaski, Emergence of self-sustained patterns in small-world excitable media, Phys. Rev. E **76**, 015101(R) (2007).

[9] Y. Qian, X. Huang, G. Hu, and X. Liao, Structure and control of self-sustained target waves in excitable small-world networks, Phys. Rev. E **81**, 036101 (2010).

[10] Y. Qian, Emergence of self-sustained oscillations in excitable Erdös-Rényi random networks, Phys. Rev. E **90**, 032807 (2014).

[11] C. Fretter, A. Lesne, C. C. Hilgetag, and M. T. Hütt, Topological determinants of self-sustained activity in a simple model of excitable dynamics on graphs, Sci. Rep. **7**, 42340 (2017).

[12] A. M. Hagerstrom, T. E. Murphy, R. Roy, P. Hövel, I. Omelchenko, and E. Schöll, Experimental observation of chimeras in coupled-map lattices, Nat. Phys. **8**, 658 (2012).

[13] I. Omelchenko, O. E. Omel'chenko, P. Hövel, and E. Schöll, When nonlocal coupling between oscillators becomes stronger: Patched synchrony or multichimera states, Phys. Rev. Lett. **110**, 224101 (2013).

[14] F. Parastesh, S. Jafari, H. Azarnoush, Z. Shahriari, Z. Wang, S. Boccaletti, and M. Perc, Chimeras, Phys. Rep. **898**, 1 (2021).

[15] Z. Lei, C. Zhang, Y. Wang, Z. Wei, Y. Qian, and Z. Zheng, Chimeralike oscillation modes in excitable scale-free networks, Phys. Rev. Res. **5**, 013006 (2023).

[16] H. Zhang, Z. Chen, F. Liu, Z. Lei, Z. Zheng, and Y. Qian, Alternate attractor chimeralike states on rings of chaotic Lorenz-type oscillators, New J. Phys. **26**, 023016 (2024).

[17] R. Q. Quiroga, J. Arnhold, and P. Grassberger, Learning driver-response relationships from synchronization patterns, Phys. Rev. E **61**, 5142 (2000).

[18] E. G. Tolkacheva, D. G. Schaeffer, D. J. Gauthier, and W. Krassowska, Condition for alternans and stability of the 1:1

response pattern in a "memory" model of paced cardiac dynamics, Phys. Rev. E **67**, 031904 (2003).

[19] M. J. E. Richardson, Firing-rate response of linear and nonlinear integrate-and-fire neurons to modulated current-based and conductance-based synaptic drive, Phys. Rev. E **76**, 021919 (2007).

[20] H. Chen, Y. Shen, Z. Hou, and H. Xin, Resonant response of forced complex networks: The role of topological disorder, Chaos **19**, 033122 (2009).

[21] D. B. Larremore, W. L. Shew, E. Ott, and J. G. Restrepo, Effects of network topology, transmission delays, and refractoriness on the response of coupled excitable systems to a stochastic stimulus, Chaos **21**, 025117 (2011).

[22] H. Grabert and M. Thorwart, Quantum mechanical response to a driven Caldeira-Leggett bath, Phys. Rev. E **98**, 012122 (2018).

[23] B. Cessac, Linear response in neuronal networks: From neurons dynamics to collective response, Chaos **29**, 103105 (2019)

[24] J. Wang, B. Deng, T. Gao, J. Wang, G. Yi, and R. Wang, Frequency-dependent response in cortical network with periodic electrical stimulation, Chaos **30**, 073130 (2020)

[25] F. T. Ndjomatchoua, C. L. Gninzanlong, T. L. M. M. Djomo, M. F. P. Kepnang, and C. Tchawoua, Enhanced signal response in globally coupled networks of bistable oscillators: Effects of mean field density and signal shape, Phys. Rev. E **107**, 064208 (2023).

[26] M. Zhan, Z. G. Zheng, G. Hu, and X. H. Peng, Nonlocal chaotic phase synchronization, Phys. Rev. E **62**, 3552 (2000).

[27] A. Bergner, M. Frasca, G. Sciuto, A. Buscarino, E. J. Ngamga, L. Fortuna, and J. Kurths, Remote synchronization in star networks, Phys. Rev. E **85**, 026208 (2012).

[28] L. V. Gambuzza, A. Cardillo, A. Fiasconaro, L. Fortuna, J. Gómez-Gardeñes, and M. Frasca, Analysis of remote synchronization in complex networks, Chaos **23**, 043103 (2013)

[29] N. Punetha, S. R. Ujjwa, F. M. Atay, and R. Ramaswamy, Delay-induced remote synchronization in bipartite networks of phase oscillators, Phys. Rev. E **91**, 022922 (2015).

[30] L. Minati, Remote synchronization of amplitudes across an experimental ring of non-linear oscillators, Chaos **25**, 123107 (2015)

[31] M. Kumar and M. Rosenblum, Two mechanisms of remote synchronization in a chain of Stuart-Landau oscillators, Phys. Rev. E **104**, 054202 (2021).

[32] Y.-S. Long, Z.-M. Zhai, M. Tang, and Y.-C. Lai, Metamorphoses and explosively remote synchronization in dynamical networks, Chaos **32**, 043110 (2022).

[33] Z. Yang, D. Chen, Q. Xiao, and Z. Liu, Phase frustration induced remote synchronization, Chaos **32**, 103125 (2022).

[34] G. Ruzzene, I. Omelchenko, J. Sawicki, A. Zakharova, E. Schöll and R. G. Andrzejak, Remote pacemaker control of chimera states in multilayer networks of neurons, Phys. Rev. E **102**, 052216 (2020).

[35] Z. Wang and Z. Liu, Effect of remote signal propagation in an empirical brain network, Chaos **31**, 063126 (2021).

[36] Q. Shen and Z. Liu, Remote firing propagation in the neural network of *C. elegans*, Phys. Rev. E **103**, 052414 (2021).

[37] Dynamic Connectome Lab, https://sites.google.com/view/dynamicconnectomelab.

[38] M. Bär and M. Eiswirth, Turbulence due to spiral breakup in a continuous excitable medium, Phys. Rev. E **48**, R1635 (1993).